Method of measuring the coupled lattice functions at the interaction point in e^+e^- storage rings

Yunhai Cai
Stanford Linear Accelerator Center, Menlo Park, California 94025, USA
(Received 26 April 2003; published 3 September 2003)

We have investigated a method of measuring the complete lattice functions including the coupling parameters at any azimuthal position in a periodic and symplectic system. In particular, the method is applied to measure the lattice functions at the interaction point where the beams collide. It has been demonstrated that a complete set of lattice functions can be accurately measured with two adjacent beam position monitors and the known transformation matrix between them. As a by-product, the method also automatically measures the complete one-turn matrix.

DOI: 10.1103/PhysRevE.68.036501 PACS number(s): 41.85.−p, 41.75.−i, 29.27.−a

I. INTRODUCTION

The lattice functions are the parameters that describe the linear motion of particles in accelerators. These functions are the well-known Courant-Snyder parameters [1] when the motion is not coupled between the horizontal and vertical planes. However, due to machine imperfections, such as the roll of quadrupole magnets or the vertical misalignment of the sextupoles, the motion is often coupled. Even in an ideal accelerator, the solenoid in a particle detector introduces coupling near the interaction point (IP). To describe the coupled particle motion, four additional parameters [2] are introduced as an extension to the Courant-Snyder parameters. Recently, it was found that another kind of parametrization [3] is necessary to complete the description of the coupled motion in accelerators, especially when the coupling is large.

Since the lattice functions completely determine the linear motion of the particles, they play an important role in the design and operation of accelerators. In particular, the vertical beta function β_y^* at the IP is one of the most important parameters in colliders because it dictates the dynamics of the beam-beam interaction during the collision process as the beam intensities increase [4]. It is well known that accurate measurement and control of β_y^* is vital to improving the luminosity.

Besides β_y^*, the tilt angle of the beam, which is strongly related to the coupling parameters, can also have measurable effects on the luminosity [5]. Therefore it is important to accurately measure the complete lattice functions including the coupling ones at the IP.

One of the best methods of measuring the lattice functions is to excite the beam coherently at the betatron frequency and then measure the phase of the oscillation at the locations of beam position monitors (BPM). This technique was first introduced at LEP for measuring the phase advances [6] and was extended for measuring coupling parameters at CESR [7]. Recently, an alternative method [8] based upon the kicking elements in the transfer matrix has been applied to the low energy ring (LER) at PEP-II [9].

All these established methods have been demonstrated to be very fast and accurate for the quantities that can be directly measured such as the phase advances between the BPMs. However, to attain indirect measurable parameters such as the β functions, some kinds of approximation are required. For example, at CESR, the relationship between the total derivative of the phase advance with respect to the independent variable s coordinate and the β function, namely, $\psi' = 1/\beta$, is valid only when the coupling is very small and hence can be neglected. Another alternative is to build a model for the entire ring. In this approach, the result depends on the choice of the fitting parameters and the time for analyzing the data could take much longer than the time for taking the data. Since the machine changes more in a longer period of time, it is hard to make a fine adjustment to the machine if the analysis time takes too long.

In this paper, we continue the investigation of the measurement technique of using the turn-by-turn BPM readings taken while the beam is coherently excited. In Secs. II and III, we start with the theory of linear coupling and a simple way to propagate the coupled lattice functions. We continue on with the description of the eigenmotion in Sec. IV and then introduce the measurement method together with a simple analytical solution in Sec. V. In Sec. VI, we study the method using realistic simulations in great detail. Finally, the estimate of the measurement errors and an actual measurement is given in Sec. VII. In Sec. VIII, we discuss the advantages and disadvantages of the method compared to others.

II. PARAMETRIZATION

Consider only the transverse motion in a circular accelerator. It has been shown by Edwards and Teng [2] that the one-turn transformation matrix $\mathbf{T}$ in a periodical and symplectic system can be decoupled by a similarity transformation

$$\mathbf{T} = \mathbf{Z} \cdot \mathbf{M} \cdot \mathbf{Z}^{-1}, \tag{2.1}$$

where $\mathbf{T}$, $\mathbf{M}$, and $\mathbf{Z}$ are all 4×4 symplectic matrices. In particular, $\mathbf{M}$ is in a block diagonal form

$$\mathbf{M} = \begin{pmatrix} M_1 & 0 \\ 0 & M_2 \end{pmatrix} \tag{2.2}$$

and $\mathbf{Z}$ is in a ''symplectic rotation'' form

$$\mathbf{Z}=\begin{pmatrix} cI & s\overline{W} \\ -sW & cI \end{pmatrix}, \tag{2.3}$$

where $M_{1,2}$, I, W, and $\overline{W}$ are all 2×2 matrices. Here I is the identity matrix and $\overline{W}$ is defined as the symplectic conjugate of matrix W, namely, $\overline{W}=-J\cdot W^T\cdot J$, where J is the unit symeplectic matrix

$$J=\begin{pmatrix} 0 & 1 \\ -1 & 0 \end{pmatrix}. \tag{2.4}$$

Moreover, the four-dimensional symplecticity requires that the submatrices $M_{1,2}$ and W are also symplectic and s,c are parametrized in terms of an angle ϕ: $s=\sin\phi$ and $c=\cos\phi$. Since each two-dimensional symplectic matrix consists of three independent parameters, it is clear from the expressions that we need ten independent parameters to describe the one-turn matrix $\mathbf{T}$.

Recently, it was shown by Sagan and Rubin [3] that there exists another solution that has the parametrization of $s=\sinh\phi, c=\cosh\phi$, and $\det(W)=-1$, instead of $s=\sin\phi, c=\cos\phi$, and $\det(W)=1$ in the previous solution. Depending upon the specific properties of $\mathbf{Z}$, one of the two solutions should be selected. We will return to them in the following section. Clearly, $\mathbf{Z}$ is related to the coupling and therefore we call ϕ the coupling angle and the elements of W as the coupling parameters in this paper. In particular, if $\phi=0$, the one-turn matrix is decoupled.

Since M_i is a symplectic matrix, it can be parametrized with the well-known Courant-Snyder parameters [1]

$$M_i=\begin{pmatrix} \cos(2\pi\nu_i)+\alpha_i\sin(2\pi\nu_i) & \beta_i\sin(2\pi\nu_i) \\ -\gamma_i\sin(2\pi\nu_i) & \cos(2\pi\nu_i)-\alpha_i\sin(2\pi\nu_i) \end{pmatrix}, \tag{2.5}$$

where ν_i is the frequency of the eigenmode, measured in units of revolution frequency. Unlike the other eight parameters of the matrix $\mathbf{T}$, one can show that $\nu_{1,2}$ are invariant, namely, independent of the locations in the ring. In addition, the symplecticity yields $\gamma_i=(1+\alpha_i^2)/\beta_i$.

Moreover, we can make another similarity transformation to the matrix M_i,

$$M_i=U_i\cdot R_i\cdot U_i^{-1}, \tag{2.6}$$

where R_i is the rotational matrix

$$R_i(2\pi\nu_i)=\begin{pmatrix} \cos(2\pi\nu_i) & \sin(2\pi\nu_i) \\ -\sin(2\pi\nu_i) & \cos(2\pi\nu_i) \end{pmatrix} \tag{2.7}$$

and

$$U_i=U_i^0=\begin{pmatrix} \sqrt{\beta_i} & 0 \\ -\alpha_i/\sqrt{\beta_i} & 1/\sqrt{\beta_i} \end{pmatrix}. \tag{2.8}$$

It is worth noting that the transformation matrix U_i is not unique. Since the rotation matrices R_i commute, it is easily seen that $U_i\cdot R(\psi_i)$, where ψ is an arbitrary angle, also satisfies Eq. (2.6). ψ_i can be interpreted as the phase for the eigenmode since it enters the equations similar to the total phase advance $2\pi\nu_i$. Here we can set ψ_i to zero because the phase itself has no physical meaning and only their differences are meaningful.

Substituting Eq. (2.6) in Eq. (2.1), we find

$$\mathbf{T}=\mathbf{A}\cdot\mathbf{R}\cdot\mathbf{A}^{-1}, \tag{2.9}$$

where

$$\mathbf{R}=\begin{pmatrix} R_1 & 0 \\ 0 & R_2 \end{pmatrix} \tag{2.10}$$

and

$$\mathbf{A}=\begin{pmatrix} cI & s\overline{W} \\ -sW & cI \end{pmatrix}\cdot\begin{pmatrix} U_1 & 0 \\ 0 & U_2 \end{pmatrix}. \tag{2.11}$$

One can see explicitly that there are eight independent parameters in the matrix $\mathbf{A}$. If we count two arbitrary phases ψ_i, $\mathbf{A}$ consists of ten independent parameters as well. In general, it can be shown that one needs only ten parameters to describe a 4×4 symplectic matrix. Based on Eq. (2.11), we can construct $\mathbf{A}$ from the lattice functions: β_i, α_i, w_a, w_b, w_c, w_d, and ϕ. Here we note that

$$W=\begin{pmatrix} w_a & w_b \\ w_c & w_d \end{pmatrix}. \tag{2.12}$$

Since $\mathbf{A}$ contains exactly the same local information as the lattice functions, it will be called the lattice matrix in this paper. Furthermore, if we have the lattice matrix $\mathbf{A}$ together with the eigentunes, we can reconstruct the one-turn matrix at that location through Eq. (2.9).

III. PROPAGATION

In principle, one could extract the lattice function directly from the one-turn matrix at any given azimuthal location in the ring based on the solutions given in Ref. [2,3]. However, the phase advances between any two positions are not well defined since at each position the analysis is independently carried out and hence the phases are arbitrary as we discussed in the preceding section.

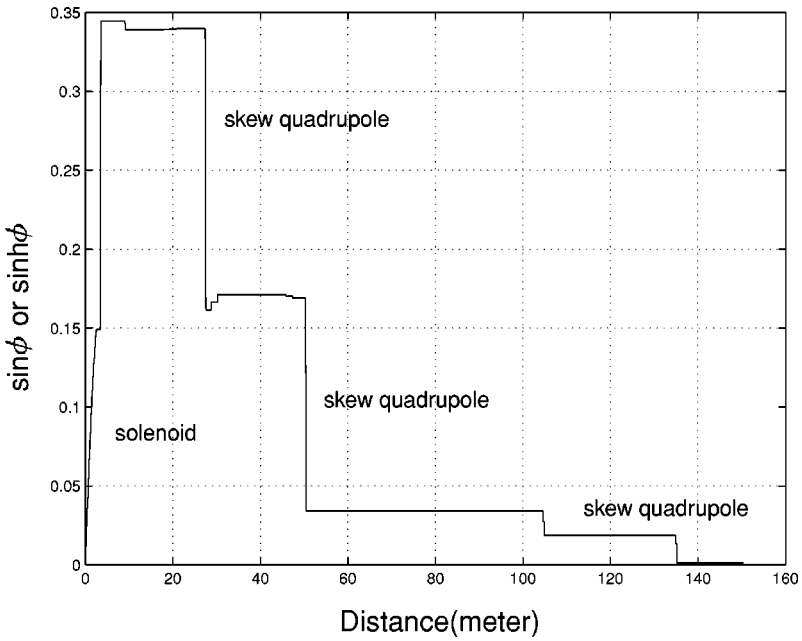

FIG. 1. Coupling angle in a half of the interaction region of the LER at PEP-II.

To resolve the ambiguity of the phase, we need to somehow relate two lattice matrices at different locations. Assuming that we have $\mathbf{A}(s_1)$ constructed from the lattice functions with zero phases at an azimuthal position s_1, we want to find a lattice matrix $\mathbf{A}(s_2)$ such that

$$\mathbf{T}(s_2)=\mathbf{A}(s_2)\cdot\mathbf{R}\cdot\mathbf{A}^{-1}(s_2), \tag{3.1}$$

where $\mathbf{T}(s_2)$ is the one-turn transformation matrix at location s_2. Please note that the rotation matrix $\mathbf{R}$ does not depend upon any azimuthal positions because the eigentunes are globally invariant quantities in this periodic system. We find that a possible solution of Eq. (3.1) is

$$\mathbf{A}(s_2)=\mathbf{T}(s_2,s_1)\cdot\mathbf{A}(s_1), \tag{3.2}$$

where $\mathbf{T}(s_2,s_1)$ is the transformation matrix from s_1 to s_2. Here we have used the concatenation property of the transformation matrices: $\mathbf{T}(s_2)=\mathbf{T}(s_2,s_1)\cdot\mathbf{T}(s_1)\cdot\mathbf{T}(s_2,s_1)^{-1}$. Equation (3.2) provides us an extremely simple way to propagate the lattice matrix around the ring.

Once we have $A(s_2)$, the lattice functions are easily extracted from it. Decomposing it in terms of 2×2 matrices

$$\mathbf{A}(s_2)=\begin{pmatrix}A_{11} & A_{12}\\ A_{21} & A_{22}\end{pmatrix} \tag{3.3}$$

and knowing $\mathbf{A}(s_2)$ is also in the form of Eq. (2.11), we find $c=\sqrt{\det A_{11}}$,

$$s=\sqrt{1-c^2},\quad s=\sin\phi(c\leqslant 1),$$

$$s=\sqrt{c^2-1},\quad s=\sinh\phi(c>1), \tag{3.4}$$

and

$$U_1=A_{11}/c,\quad U_2=A_{22}/c,\quad W=-A_{21}\cdot U_1^{-1}/s. \tag{3.5}$$

The Courant-Snyder parameters and the phase advances can be calculated using

$$\beta_i=U_i(1,1)^2+U_i(1,2)^2,$$

$$\alpha_i=-[U_i(1,1)U_i(2,1)+U_i(1,2)U_i(2,2)],$$

$$\gamma_i=U_i(2,1)^2+U_i(2,2)^2,$$

$$\delta\psi_i=\tan^{-1}[U_i(1,2)/U_i(1,1)]. \tag{3.6}$$

These formulas are derived from the fact that U_i is equivalent to $U_i\cdot R(\theta)$, where θ is an arbitrary angle. In particular, by choosing $\theta=-\delta\psi_i$, we can cast U_i into the form of Eq. (2.8). Here $\delta\psi_i$ is now well defined as the phase difference between s_1 and s_2 if the phase at s_1 is set to zero.

This formulation of calculating lattice functions has been coded numerically in LEGO [10]. The coupling angle in a half of the interaction region in the LER is plotted in Fig. 1. One can see from the figure, the maximum ϕ is as large as 20°. Indeed, for such a large coupling, both solutions of parametrization are required to make a complete calculation in the region.

Here we plot ϕ to show its important properties: It can be changed only by coupling elements such as skew quadrupole or solenoid. As a result, we can clearly see the steps where the skew quadrupoles and solenoid are located in the region.

As a concrete example, let us consider two positions in the ring when the space between them is a drift space of length L. The transfer matrix for the drift is written as

$$\mathbf{T}_d=\begin{pmatrix}1 & L & 0 & 0\\ 0 & 1 & 0 & 0\\ 0 & 0 & 1 & L\\ 0 & 0 & 0 & 1\end{pmatrix}. \tag{3.7}$$

It is straightforward to derive the lattice functions at the end of the drift space explicitly in terms of those at the beginning. Denoting all quantities at the end with tilde, the Courant-Snyder parameters are given by

$$\tilde{\beta}_{1,2}=[L^2+(\beta_{1,2}-L\alpha_{1,2})^2]/\beta_{1,2},$$

$$\tilde{\alpha}_{1,2}=\alpha_{1,2}-L\gamma_{1,2},$$

$$\tilde{\gamma}_{1,2}=\gamma_{1,2}, \tag{3.8}$$

the phase advance

$$\delta\psi_{1,2}=\tan^{-1}[L/(\beta_{1,2}-L\alpha_{1,2})], \tag{3.9}$$

the coupling parameters

$$\tilde{w}_a=w_a+w_cL,$$

$$\tilde{w}_b=w_b-L(w_a-w_d+w_cL),$$

$$\tilde{w}_c=w_c,$$

$$\tilde{w}_d=w_d-w_cL, \tag{3.10}$$

and $\tilde{\phi}=\phi$. One can see that, in this simple example of the drift space, the Courant-Snyder parameters and the coupling parameters propagate independently. However, it is evident that it is not true for a more general transformation.

IV. EXCITED EIGENMOTION

An eigenmode can be excited in an electron ring by a continuing driving kick at the frequency of the mode [6]. Balancing this with the radiation damping, a steady state is reached after a few damping times. At the saturated state, the turn-by-turn readings by a perfect BPM can be derived [11] directly from the lattice matrix A in Eq. (2.11), which transfers the eigencoordinates to physical ones. With only the excited eigenmode 1, we have

$$x_n^{(1)}=K_1c\sqrt{\beta_1}\sin(2\pi n\nu_1+\psi_1),$$

$$y_n^{(1)}=-K_1s\sqrt{J_1(w_a,w_b)}\sin(2\pi n\nu_1+\psi_1+\delta\mu_1), \tag{4.1}$$

where $J_1(w_a,w_b)=\beta_1w_a^2-2\alpha_1w_aw_b+\gamma_1w_b^2$ and

$$\sin(\delta\mu_1)=\frac{w_b}{\sqrt{\beta_1J_1(w_a,w_b)}},$$

$$\cos(\delta\mu_1)=\frac{w_a\beta_1-w_b\alpha_1}{\sqrt{\beta_1J_1(w_a,w_b)}}. \tag{4.2}$$

K_1 is the amplitude of the excitation which is a global quantity, meaning that it is the same at all BPMs. ψ_1 is the betatron phase of the eigenmode 1. It is well known that the difference ψ_1 between the BPMs gives us the phase advance. Here the subscript n is the index of the turns.

Since mode 1 mostly oscillates in the horizontal plane when the coupling is weak, we sometime call $x_n^{(1)}$ in Eq. (4.1) the ''in-plane'' and $y_n^{(1)}$ the ''out-plane'' oscillation. Notice that there is a phase shift $\delta\mu_1$ between the in-plane and out-plane oscillation. In addition, one can show that $J_1(w_a,w_b)$ is always positive and therefore it is sometime called the out-plane β function.

Similarly, if only mode 2 is excited, we have

$$x_n^{(2)}=K_2s\sqrt{J_2(w_d,w_b)}\sin(2\pi n\nu_2+\psi_2+\delta\mu_2),$$

$$y_n^{(2)}=K_2c\sqrt{\beta_2}\sin(2\pi n\nu_2+\psi_2), \tag{4.3}$$

where $J_2(w_d,w_b)=\beta_2w_d^2+2\alpha_2w_dw_b+\gamma_2w_b^2$ and

$$\sin(\delta\mu_2)=-\frac{w_b}{\sqrt{\beta_2J_2(w_d,w_b)}},$$

$$\cos(\delta\mu_2)=\frac{w_d\beta_2+w_b\alpha_2}{\sqrt{\beta_2J_2(w_d,w_b)}}. \tag{4.4}$$

It is obvious that these two sets of turn-by-turn readings at a single BPM are still not enough to determine the complete eight parameters of lattice functions at that location because the quantities associated with the slope could not be measured at a single position.

V. AN ANALYTICAL SOLUTION

Since the slope is the concern, it is natural to add the next BPM into the measurement system. For simplicity, let us consider a system of two BPMs connected by a drift space with length L. As an example shown in Sec. III, the lattice functions at the second BPM are completely determined by the initial functions at the first BPM and the length of the drift. The analytical expressions are given in Eqs. (3.8)–(3.10).

Suppose we have recorded the two sets of turn-by-turn readings at the two BPMs taken when the eigenmotion is excited separately in modes 1 and 2 as described in the preceding section; we want to find the complete lattice functions at the entry in terms of the readings. First, we can easily obtain the amplitudes of the oscillations and then extract the phases of the oscillations by using a fast Fourier transformation. Taken together, we have eight phases and eight amplitudes. Finally, we would like to solve the lattice functions in terms of these 16 parameters. Of course, not all 16 parameters are independent because of the symplecticity.

Here we continue to note the quantities at the exit or the second BPM with tilde. When mode 1 is excited, the in-plane amplitudes $x_n^{(1)}$ and $\tilde{x}_n^{(1)}$ are proportional to the excitation amplitude K_1 as indicated in Eq. (4.1). Knowing that ϕ is not changed by a drift, we can take the ratio κ_1 of the amplitudes and obtain

$$\beta_1/\tilde{\beta}_1=\kappa_1^2, \tag{5.1}$$

according to Eq. (4.1).

On the other hand, combining the first equation in Eqs. (3.8) with Eq. (3.9), we have

$$\beta_1\tilde{\beta}_1 = L^2(1+\cot^2\delta\psi_1), \tag{5.2}$$

where $\delta\psi_1 = \tilde{\psi}_1 - \psi_1$. The above two equations are easily solved. We find

$$\beta_1 = L|\kappa_1 \csc\delta\psi_1|,$$

$$\tilde{\beta}_1 = L|\csc\,\delta\psi_1|/|\kappa_1|. \tag{5.3}$$

Similarly, for mode 2, we have

$$\beta_2 = L|\kappa_2 \csc\delta\psi_2|,$$

$$\tilde{\beta}_2 = L|\csc\,\delta\psi_2|/|\kappa_2|, \tag{5.4}$$

where κ_2 is ratio of the vertical amplitudes while the second mode is excited. Substituting the solution of $\beta_{1,2}$ back into Eq. (3.9), we obtain

$$\alpha_{1,2} = |\kappa_{1,2}\csc\,\delta\psi_{1,2}| - \cot\,\delta\psi_{1,2}. \tag{5.5}$$

Finally $\tilde{\alpha}_{1,2}$ is solved by simply using the second equation in Eqs. (3.8).

Once the Courant-Snyder parameters are known, we are in a position to solve the coupling parameters, w_a, w_b, w_c, w_d, by using the measured out-plane phases, $\delta\mu_1$, $\delta\mu_2$, and $\delta\tilde{\mu}_1$. First, we express w_a, w_c, and w_d in terms of w_b using Eqs. (4.2) and (4.4)

$$w_a = w_b(\alpha_1 + \cot\,\delta\mu_1)/\beta_1,$$

$$w_d = -w_b(\alpha_2 + \cot\,\delta\mu_2)/\beta_2, \tag{5.6}$$

and $w_c = (w_a w_d - 1)/w_b$ for the first kind of solution. Then we substitute them into Eq. (3.10) to obtain the coupling parameters, $\tilde{w}_a$ and $\tilde{w}_b$ at the exit. Finally we solve w_b from the equation

$$\tilde{w}_a = \tilde{w}_b(\tilde{\alpha}_1 + \cot\,\delta\tilde{\mu}_1)/\tilde{\beta}_1. \tag{5.7}$$

It is straightforward to find

$$w_b = \pm L\sqrt{|\csc\,\delta\psi_1 \csc\,\delta\psi_2|F_1F_2}, \tag{5.8}$$

where

$$F_1 = \kappa_1\csc(\delta\psi_1 + \delta\tilde{\mu}_1 - \delta\mu_1)\sin(\delta\mu_1)\sin(\delta\psi_1 + \delta\tilde{\mu}_1),$$

$$F_2 = \kappa_2\csc(\delta\mu_2 - \delta\psi_2)\sin(\delta\mu_2)\sin(\delta\psi_2). \tag{5.9}$$

In addition, it is easily seen that the coupling angle ϕ is given by

$$\tan\phi = (\sqrt{\beta_1\beta_2/(J_1J_2)}/\kappa_{12}\kappa_{21})^{1/2}, \tag{5.10}$$

where κ_{12} and κ_{21} are the ratios of the in-plane amplitude to the out-plane one while mode 1 or 2 is excited.

TABLE I. The lattice functions at the IP of the LER using three different approaches. The results in the second column are obtained with the procedure outlined in Secs. II and III. The third column is the result of a direct fitting to the turn-by-turn readings of two BPMs. In the fourth column, we extract the phases and amplitudes from the data and then use the analytical formulas in this section for computing the lattice functions.

Parameter at the IP	Calculation	Numerical	Analytical
β_1^* (m)	0.5332	0.5327	0.5383
α_1^*	−0.0986	−0.0943	−0.0944
β_2^*(m)	0.0172	0.0174	0.0174
α_2^*	−0.0125	−0.0158	−0.0062
$\sinh\phi^*$	0.0671	0.0667	0.0662
w_a^*	−0.1684	−0.1720	−0.1743
w_b^* (m)	0.0492	0.0510	0.0488
w_c^* (m^{-1})	6.9911	6.7903	6.8149
w_d^*	3.8807	3.7986	3.8291

For the second kind of solution, the exact same derivation goes through except that we have $w_c = (w_a w_d + 1)/w_b$. The solution becomes

$$w_b = \pm L\sqrt{-|\csc\,\delta\psi_1 \csc\,\delta\psi_2|F_1F_2} \tag{5.11}$$

and

$$\tanh\phi = \sqrt{\sqrt{\beta_1\beta_2/(J_1J_2)}/\kappa_{12}\kappa_{21}}. \tag{5.12}$$

The choice of what kind of solutions to use in the analysis is determined entirely by the sign of F_1F_2. If $F_1F_2 > 0$, we choose the first solution because w_b should be a real number in the stable system. In the other case, the second solution should be chosen.

Of course, instead of using $\delta\tilde{\mu}_1$, one could also use $\delta\tilde{\mu}_2$ to solve the coupling parameters. In practice, we find that they yield the same numerical results.

In addition, we want to apply the results to measure the lattice functions including the coupling parameters at the IP. For simplicity, let us assume that the IP is halfway between the two BPMs. Since we know the lattice functions at the beginning, the functions at the middle are easily obtained by propagating a half of the distance in the drift. We have

$$\beta_{1,2}^* = L[2|\kappa_{1,2}|\cot\,\delta\psi_{1,2} + (1+\kappa_{1,2}^2)|\csc\,\delta\psi_{1,2}|]/4|\kappa_{1,2}|,$$

$$\alpha_{1,2}^* = (\kappa_{1,2}^2 - 1)|\csc\,\delta\psi_{1,2}|/2|\kappa_{1,2}|. \tag{5.13}$$

As a reminder, here L is the length and $\delta\psi_{1,2}$ are the phase advances between the two BPMs.

To compare this analytical solution with the theoretical calculation and the direct numerical fitting to the simulated data (to be discussed in the following section in detail) we study a few cases where the solenoid is turned off. The result of a typical one is tabulated in Table I. In the table, we have summarized the lattice functions derived from three different approaches: calculation, numerical fitting, and analytical solution. One can see that the agreements are excellent.

Here we have derived the complete set of lattice functions at a given azimuthal location in the ring in terms of the ratios of amplitudes and phase differences of the coherent oscillations. As we mentioned at the end of Sec. II, the lattice matrix can be constructed based on Eq. (2.11) with the complete lattice functions. Therefore, together with the measured eigentunes, we can automatically measure the one-turn matrix using Eq. (2.9).

For a symmetric final focusing system, $|\kappa_{1,2}|=1$ and thus $\alpha^*_{1,2}=0$. The β functions are further simplified to

$$\beta^*_{1,2}=L(\cot\delta\psi_{1,2}+|\csc\delta\psi_{1,2}|)/2. \tag{5.14}$$

Often this formula gives an excellent estimate of β^* assuming the beam waist is halfway between the two BPMs even when a solenoid is present because the focusing effects by the solenoid are rather weak in high-energy accelerators. For example, if we apply this simple formula to the phase advance data taken recently from the rings at PEP-II, we have $\beta^*_x=33.8$ cm and $\beta^*_y=1.24$ cm in the LER and $\beta^*_x=40.64$ cm and $\beta^*_y=1.15$ cm in the high-energy ring. These values of the β functions are consistent with the results attained by other types of measurement.

VI. SIMULATION

In general, it is hard to solve explicitly the lattice functions if the space between two BPMs is not a drift. Still, we would like to extend the method at least numerically to more general situations, more importantly, to a solenoid that usually covers the vicinity of the IP.

To make a realistic simulation, we continue to build up the class library LEGO [10] and add a new type of kicker into the code. The kicker is allowed to periodically excite the beam either in the horizontal or vertical plane with a sinusoidal wave locked at a certain frequency.

In the simulation, we build a realistic LER model including a solenoid in a particle detector. Typically, after assigning systematic and random errors into the design lattice, we steer the orbit, make coupling corrections, and adjust the tunes to the working point. After the model is ready for taking the simulated data, we first analyze the lattice functions in the entire ring relative to the closed orbit, using the method we have outlined in Sec. III. In particular, we calculate the lattice functions at the IP so that they can be compared with the simulated measurements.

To make a simulated measurement, we first switch on the radiation so that the particle will lose energy while it passes through the magnets according to the standard formula [12]. In addition, the phases of the cavities are set at the proper values such that the energy lost per turn is exactly compensated. It is well known that the process of a particle losing energy in the magnets and then gaining back the energy in the cavities results in radiation damping.

Moreover, we turn on the kicker that is locked on the frequency of mode 1 to periodically kick the beam in the horizontal plane. The particle is tracked up to four damping times, about 40 000 turns, until it reaches the saturated amplitude at which point the excitation is being balanced by the radiation damping. We continuously record the transverse beam positions at the IP and its two adjacent BPMs for 1024 turns. For the second set of data, we repeat the same process while locking on the frequency of mode 2 and excite the beam in the vertical plane. The two BPMs used here are 72 cm away from the IP and inside the solenoid.

The two sets of simulated data are plotted in Fig. 2 in blue at three different locations in the sequence defined by the direction of the beam. In the middle row are the readings at the IP. Since there is no real BPM at the IP in the machine, we display them here only for the purpose of illustration. The left column displays the first set of data taken while mode 1 is excited and the right column for the second set. It can be seen in the figure that the readings trace out titled ellipses in all cases since the oscillations being driven always have the same frequency as the driving force.

Given the simulated data, we know theoretically that they can be described by $x^{(i)}_n$ and $y^{(i)}_n$ in Eqs. (4.1) and (4.3). Mathematically, that means that we may define the function χ^2 to be minimized with least-square fitting

$$\chi^2=\frac{1}{2}\sum_{n=1,1024}^{i=1,2}[(x^{(i)}_n-X^{(i)}_n)^2+(y^{(i)}_n-Y^{(i)}_n)^2+(\tilde{x}^{(i)}_n-\tilde{X}^{(i)}_n)^2 + (\tilde{y}^{(i)}_n-\tilde{Y}^{(i)}_n)^2], \tag{6.1}$$

where $X^{(i)}_n$ and $Y^{(i)}_n$ are the actual turn-by-turn readings and the tilde notes the corresponding quantities at the second BPM. Here we required all eight oscillations at both BPMs to be fitted simultaneously.

Since the lattice functions, including the phase advances at the second BPM, can be derived from the initial lattice functions at the first BPM, if the transformation matrix is known, they are eliminated as independent fitting variables. Only their derived values are used in the fitting.

In the LER, we extract the transformation matrix between two BPMs from the prepared lattice, as if it is known exactly. This assumption is partially justified because there are no strong focusing elements in between. In this particular case, the elements include only the solenoid and bending magnets.

With the transformation matrix, we finally reduce the number of independent fitting variables to 22. They include $\beta_{1,2}$, $\alpha_{1,2}$, sw_a, sw_b, sw_c, sw_d, $\psi_{1,2}$, $\nu_{1,2}$, $K_{1,2}$, and eight parameters that specify the centers of the ellipses. The fitted result is shown in Fig. 2 in green color. One can see from the figure that the fitting is in excellent agreement with the data. The residuals are reduced below 10 μm.

Once we have the fitted initial lattice functions at the entry, we propagate them to the IP. The propagated functions are tabulated in Table II, in addition to these values from the direct calculation before the data is taken. Based on the propagated lattice functions, we compute the eigen motions according to Eqs. (4.1) and (4.3) at the IP and show them in Fig. 2 in red in the middle row. It is clear from the figure that the direct simulation is consistent with the prediction based on the numerical measurement at the IP.

The results in Fig. 2 and Table II are those from a typical case among many random seeds that we have studied. To demonstrate this, we show β^*_2 and ϕ^* from all seeds that

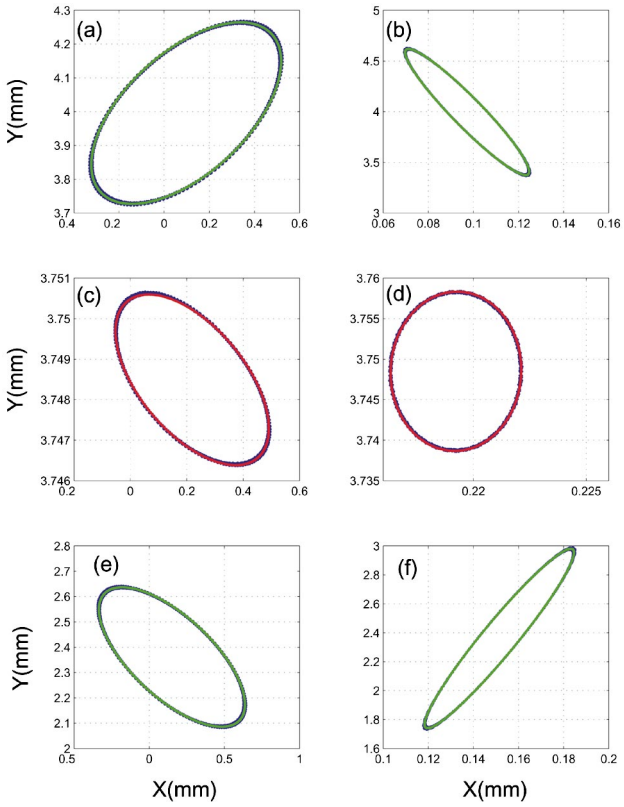

FIG. 2. (Color) Simulated turn-by-turn measurement at two BPMs near the IP in the LER: (a) and (b) represent the readings of the first BPM when the beam is excited in the horizontal and vertical plane, respectively, (c) and (d) for the IP, and (e) and (f) for the second BPM.

have been studied in Fig. 3. In all these cases, any information related to the specific seed is never used in the fittings. For example, the initial lattice functions at the beginning of the fitting are always set at their design values.

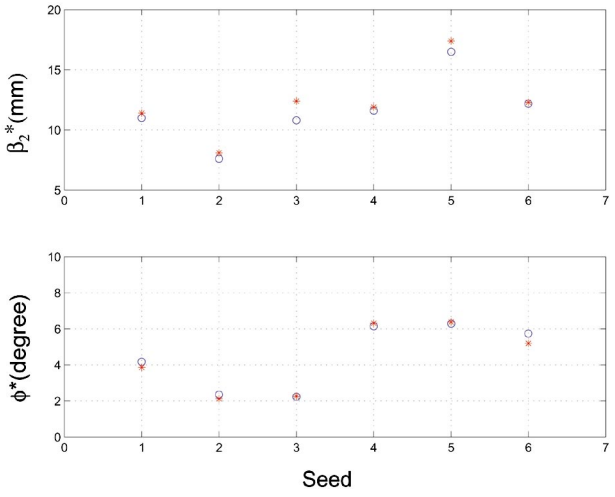

FIG. 3. (Color) Measurement of lattice functions at the IP. The circles represent the calculated values and the stars represent the numerically measured ones.

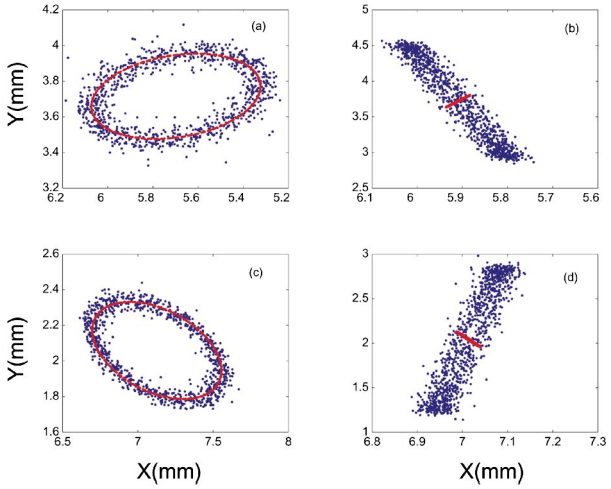

FIG. 4. (Color) Turn-by-turn measurement at two BPMs near the IP in the LER: (a) and (b) represent the data of the first BPM when the beam is excited in the horizontal and vertical plane, respectively, and (c) and (d) for the second BPM.

VII. MEASUREMENT

Up to this point we have assumed that the BPMs are perfect and therefore we have no errors in the measurements. However, it is well known that the actual readings of a BPM can be distorted by the errors in its geometry and electronics. Since the errors are largely compensated with good calibration, we assume that the errors are small and thus linear. The actual transverse positions of the beam described by $x_n^{(i)}$ and $y_n^{(i)}$ are scaled linearly

$$X_n^{(i)} = g_x x_n^{(i)} + g_{yx} y_n^{(i)},$$

$$Y_n^{(i)} = g_{xy} x_n^{(i)} + g_y y_n^{(i)}, \tag{7.1}$$

to generate the real readings $X_n^{(i)}$ and $Y_n^{(i)}$. $g_{x,y}$ are commonly called the gain and $g_{xy,yx}$ the cross coupling for the BPMs.

TABLE II. Numerical measurement of the lattice function at the IP. The results in the second column are obtained with the method outlined in Secs. II and III. The third column is the result of a direct fitting to the turn-by-turn readings of two BPMs described in this section.

Parameter at the IP	Calculation	Numerical
β_1^* (m)	0.5258	0.5253
α_1^*	0.1459	0.1520
β_2^* (m)	0.0110	0.0114
α_2^*	−0.0900	−0.0927
$\sinh\phi^*$	0.0728	0.0674
w_a^*	0.0398	0.0511
w_b^* (m)	−0.0522	−0.0497
w_c^* (m^{-1})	−18.2750	−19.7770
w_d^*	−0.9313	−0.3235

It is obvious that these unknown errors will cause some systematic errors in the measurement. For simplicity, let us now assume that $g_{xy}=g_{yx}=0$ and the space between the two BPMs is a drift. With this simplification, we can repeat the similar exercise as we did in Sec. V and find the analytical solution. It is easily seen that the results are obtained simply by replacing $\kappa_{1,2}$ with $\kappa_{1,2}\tilde{g}_{x,y}/g_{x,y}$ in all the equations in Sec. V. In particular, we have

$$\beta^*_{1,2}=L[2|\bar{\kappa}_{1,2}|\cot\delta\psi_{1,2}+(1+\bar{\kappa}^2_{1,2})|\csc\delta\psi_{1,2}|]/4|\bar{\kappa}_{1,2}|,$$

$$\alpha^*_{1,2}=(\bar{\kappa}^2_{1,2}-1)|\csc\delta\psi_{1,2}|/2|\bar{\kappa}_{1,2}|, \tag{7.2}$$

where $\bar{\kappa}_{1,2}=\kappa_{1,2}\tilde{g}_{x,y}/g_{x,y}$. Note that only the ratio of the gains enters the solution. The reason for that is that the symmetric part of the gains can always be absorbed by the global oscillation amplitudes $K_{1,2}$.

The errors of β^*_i and α^*_i in the measurements can also be estimated directly using Eq. (5.13) and taking their partial derivatives with respect to the variables κ_i and $\delta\psi_i$. For β^*_i, we write

$$\frac{\Delta\beta^*_i}{\beta^*_i}=\left[\frac{(\kappa_i^2-1)|\csc\delta\psi_i|}{2|\kappa_i|\cot\delta\psi_i+(1+\kappa_i^2)|\csc\delta\psi_i|}\right]\frac{\Delta|\kappa_i|}{|\kappa_i|}. \tag{7.3}$$

The equation shows that β^*_i is most insensitive to the error caused by the ratio of the amplitudes since κ_i is always near 1 in existing colliders. However, there is one exception, that is, when csc $\delta\psi_i$ becomes infinity, which could happen as β^*_i approaches zero. Normally $\beta^*_y\ll\beta^*_x$ in electron storage rings; this means that β^*_y is much more sensitive than β^*_x with respect to the errors in the ratio of the amplitudes.

For α^*_i, we find

$$\frac{\Delta\alpha^*_i}{\alpha^*_i}=\frac{\kappa_i^2+1}{\kappa_i^2-1}\frac{\Delta|\kappa_i|}{|\kappa_i|}. \tag{7.4}$$

The pole at $|\kappa_i|=1$ in the coefficient implies that α_i is extremely sensitive to the errors in κ_i.

For symmetric colliders, we use Eq. (5.14) to make an estimate of measurement errors in β^*_i. The accuracy required in the measurement of the phase advance ψ_i is given by

$$\frac{\Delta\beta^*_i}{\beta^*_i}=-|\csc\delta\psi_i|\Delta\psi_i. \tag{7.5}$$

Since smaller β^*_i makes $\delta\psi_i$ closer to π, the equation implies that the measured β^*_i grows more uncertain as β^*_i becomes smaller. This phenomenon was seen recently at PEP-II when β^*_y was lowered. Given the same errors in the phase advances, the equation also shows that the measured β^*_x is more accurate than β^*_y if $\beta^*_x>\beta^*_y$.

In the general case, we have simulated extensively the effects of these systematic errors on the accuracy of the measurement in realistic lattices with the solenoid. In the simulation, the BPM errors are assigned to the their readings according to Eqs. (7.1). In the numerical studies, we find that the dependencies of the BPMs gains in β^*_i and α^*_i are very similar to their analytical estimates. That is not surprising because the focusing effects from the solenoid are so weak that it can be ignored in high-energy accelerators.

One may consider using the gains as additional fitting variables. In this approach, we find that β^*_i and α^*_i become arbitrary, although there is always a good fit to the data. In other words, this simple measurement system cannot separate the gains from the lattice functions.

Similar conclusions can be reached when cross couplings are present in the measurement, except that they mainly affect the accuracy of the coupling parameters instead of the Courant-Snyder parameters. We find only one exceptional case in which we can separate the cross couplings from the lattice functions, that is, where there exists cross couplings in only one of the two BPMs and we use them as the fitting variables. Of course, there is no way to know this information in an actual measurement and it is therefore not very useful.

In general, we find that the BPM errors should not be used as fitting variables and should be limited to less than 0.1% in order to achieve 10% accuracy in the measurement. Of course, the random noise could also contribute to the errors in the measurement. We find that it should also be reduced below 0.1%. These requirements are rather stringent compared to the BPM system we have at PEP-II. Nevertheless, it is still interesting to see how the method can be applied to the actual data from the measurement.

Here we take a look at the data taken recently during a machine development in the LER. The real data are much noisier than the one generated from the simulation. A square filter near the peak in the frequency domain is used to clean up the data. After the filtering, the data at the same two BPMs as in the simulation are shown in Fig. 4 in blue color. It is clearly seen from the data in the right column that the random noise in the horizontal plane smears the ellipses excited by mode 2. As a result, the ellipses become parallelograms.

We fit the data exactly the same way as in the simulation. The fitted points are plotted in Fig. 4 in red. One can see that the fit for mode 1 is good but is not so for mode 2, probably due to the noise.

The result of the measurement at the IP is tabulated in Table III and compared with the design values. It is not clear how accurate the measured results are in the table, given the unknown gains and cross couplings in the BPMs. We expect that the lattice functions are much more accurate in the horizontal plane than the vertical one, based on the previous error analysis and the residual of the fitting.

It is surprising to see that β^*_2 is not so far away from its design value, given the inadequate fit. That is most likely due to the constraints on the phases. The measurement of α^*_2 indicates that the errors of the vertical gain are probably very large because the derived vertical beam waist, $s_w\approx\alpha^*_2\beta^*_2\approx 8$ mm, is more than half of the bunch length, which is very unlikely since the degradation of the luminosity from such a large shift of the waist is not seen at PEP-II. Assuming the beam waist is actually in the middle, we estimate that the

TABLE III. Measurement of a complete set of lattice functions including the coupling parameters at the IP.

Parameter at the IP	Design values	Measured values
β_1^* (m)	0.5000	0.2415
α_1^*	0.0000	0.2447
β_2^* (m)	0.0125	0.0167
α_2^*	0.0000	0.4642
$\sin\phi^*$	0.0014	0.6145
w_a^*	0.1428	−0.0189
w_b^* (m)	0.1428	−0.3358
w_c^* (m^{-1})	−7.0000	2.9913
w_d^*	0.3571	0.2428

vertical BPM gains have errors of about 2%. Similarly, we can show that the measured couplings are too large compared to the vertical beam size obtained indirectly from the luminosity scan. It implies that the cross coupling from the BPM is also too large in the measurement. Although only one set of data is shown here, the results from many other datasets are very similar.

VIII. DISCUSSION

A new method of measuring the lattice functions at any azimuthal position in a periodic and symplectic system, including the coupling parameters, is studied in great detail. In particular, the method is applied to measure the lattice functions at the IP where the beams collide. We have demonstrated numerically that a complete set of lattice functions can be accurately measured using two adjacent BPMs together with the known transformation matrix between them.

With an example of drift space, we analytically solved the lattice functions in terms of the phase differences and ratios of amplitudes of the excited oscillations. For this example, the analytical and numerical solutions yield essentially identical results. Based on the analytical formula, estimates of the measurement errors due the systematic errors are given as well.

This method has been applied to the LER at PEP-II. As one may expect, the measured lattice functions at the IP are not accurate enough partially because of the large gain and cross couplings in the two neighboring BPMs. An order of magnitude improvement in the BPM reading accuracy is required to obtain any meaningful measurement of the coupling and beam waist near the IP. Although the BPMs are not yet accurate enough to measure the complete set of lattice functions at the IP in the LER, the estimates of β_i^* using only the phase advances are still quite useful.

The disadvantage of this method is clearly demonstrated when it is applied to the actual measurement because of relatively large uncertainties in the amplitudes compared to the phases. That is the reason why the method of the phase advance [7] is so widely used in existing accelerators including PEP-II. It is not clear yet how to use only the phase to measure locally the coupling at the IP.

Although it is very difficult, if not impossible, to improve by an order of magnitude for the accuracy of BPM readings in the entire ring, it is not so difficult if one considers only two special ones near the IP. Should one achieve the required accuracy, the measurement and analysis could be carried on within 1 min. Then one could even use it in an active feedback system to control the beam distribution at the IP.

In addition, we can apply the method separately to two given locations in the ring and obtain the lattice matrices $\mathbf{A}(s_1)$ and $\mathbf{A}(s_2)$. Then we can derive the complete transformation matrix between the two points using Eq. (3.2).

ACKNOWLEDGMENTS

The author would like to thank Stan Ecklund and Mike Sullivan for taking the data and Martin Donald, John Irwin, John Seeman, Uli Wienands, and especially Franz-Josef Decker and Yiton Yan for many helpful discussions. This work was supported by the Department of Energy under Contract No. DE-AC03-76SF00515.

[1] E.D. Courant and H.S. Snyder, Ann. Phys. **3**, 1 (1958).
[2] D.A. Edwards and L.C. Teng, IEEE Trans. Nucl. Sci. **20**, 885 (1973).
[3] D. Sagan and D. Rubin, Phys. Rev. ST Accel. Beams **2**, 074001 (1999).
[4] R.H. Siemann, SLAC-PUB Report No. 6073, 1993 (unpublished).
[5] Y. Cai, in *Luminosity of Asymmetric e^+e^- Collider with Coupling Lattice*, Proceedings of the Seventh EPAC, Vienna, Austria, 2000, edited by J.-L. Laclare, W. Mitarroff, Ch. Petit-Jean-Genaz, J. Poole, and M. Regler (Austrian Academy of Science Press, Vienna, 2000), p. 400.
[6] J. Borer, C. Bovet, A. Burns, and G. Morpurgo, in ''Harmonic Analysis of Coherent Bunch Oscillations in LEP,'' Proceedings of the Third EPAC, Berlin, Germany, 1992, p. 1082.
[7] D. Sagan, R. Miller, R. Littauer, and D. Rubin, Phys. Rev. ST Accel. Beams **3**, 092801 (2000).
[8] J. Irwin and Y.T. Yan, in *Beamline Model Verification Using Model Independent Analysis*, Proceedings of the Seventh EPAC, Vienna, Austria, 2000 (Ref. [5]), p. 151.
[9] J. Dorfan and M. Zisman, SLAC Report No. 418, 1993 (unpublished).
[10] Y. Cai, M. Donald, J. Irwin, Y. Yan, SLAC-PUB Report No. 7642, 1997 (unpublished).
[11] P. Bagley and D. Rubin, in *Correction of Transverse Coupling in a Storage Ring*, Proceedings of the PAC, Chicago, Illinois, 1989, edited by F. Bennett and J. Kopta (IEEE, New York, 1989), p. 874.
[12] M. Sands, SLAC-Report No. 121, 1979 (unpublished).